

# A General Theoretical Framework to Infer Endosomal Network Dynamics from Quantitative Image Analysis

Lionel Foret,<sup>1,2,6</sup> Jonathan E. Dawson,<sup>1,6</sup> Roberto Villaseñor,<sup>3,6</sup> Claudio Collinet,<sup>3</sup> Andreas Deutsch,<sup>4</sup> Lutz Brusch,<sup>4</sup> Marino Zerial,<sup>3</sup> Yannis Kalaidzidis,<sup>3,5</sup> and Frank Jülicher<sup>1,\*</sup>

<sup>1</sup>Max Planck Institute for the Physics of Complex Systems, Nöthnitzer Straße 38, 01187 Dresden, Germany

<sup>2</sup>Laboratoire de Physique Statistique, Ecole Normale Supérieure, UPMC, CNRS, 24 rue Lhomond, 75005 Paris, France

<sup>3</sup>Max Planck Institute of Molecular Cell Biology and Genetics, Pfotenhauer Straße 108, 01307 Dresden, Germany

<sup>4</sup>Center for Information Services and High Performance Computing (ZIH), Technische Universität Dresden, Nöthnitzer Strasse 46, 01187 Dresden, Germany

<sup>5</sup>Belozersky Institute of Physico-Chemical Biology, Moscow State University, 119899 Moscow, Russia

## Summary

**Background:** Endocytosis allows the import and distribution of cargo into a series of endosomes with distinct morphological and biochemical characteristics. Our current understanding of endocytic cargo trafficking is based on the kinetics of net cargo transport between endosomal compartments without considering individual endosomes. However, endosomes form a dynamic network of membranes undergoing fusion and fission, thereby continuously exchanging and redistributing cargo. The macroscopic kinetic properties, i.e., the properties of the endosomal network as a whole, result from the collective behaviors of many individual endosomes, a problem so far largely unaddressed.

**Results:** Here, we developed a general theoretical framework to describe the dynamics of cargo distributions in the endosomal network. We combined the theory with quantitative experiments to study how the macroscopic kinetic properties of the endosomal network emerge from microscopic processes at the level of individual endosomes. We compared our theory predictions to experimental data in which dynamic distributions of endocytosed low-density lipoprotein (LDL) were quantified.

**Conclusions:** Our theory can quantitatively describe the observed cargo distributions as a function of time. Remarkably, the theory allows determining microscopic kinetic parameters such as the fusion rate between endosomes from still images of cargo distributions at different times of internalization. We show that this method is robust and sensitive because cargo distributions result from an average over many stochastic events in many cells. Our results provide theoretical and experimental support to the “funnel model” of endosome progression and suggest that the conversion of early to late endosomes is the major mode of LDL trafficking.

## Introduction

Cells communicate with their environment by taking up and secreting many different metabolites and signaling molecules [1–4]. Several molecules selectively and efficiently enter the cell in a process called receptor mediated endocytosis (RME). In this process, a ligand binds specifically to its receptor(s) at the plasma membrane and is subsequently internalized into the cell mostly via clathrin coated vesicles (CCV). Upon CCV fusion with early endosomes, cargo enters a dynamic network of early endosomes [5] where ligands and receptors are sorted and transported to their final destination [4]. Cargo molecules leave the early endosomal network either by recycling to the cell surface or by entering a network of late endosomes and lysosomes, where cargo is degraded. For example, transferrin is recycled to the cell surface from early endosomes, whereas low-density lipoprotein (LDL) is transported to late endosomes and lysosomes for degradation [6]. The function of endosomes in sorting and trafficking is governed by the dynamic assembly on the membrane of a multiprotein machinery organized by small GTPases of the Rab family. Rab proteins specify the function of distinct intracellular compartments [7–11], e.g., early endosomes are characterized by Rab5 [5, 12] and late endosomes by Rab7 [5] and their respective effectors. Rab5-positive early endosomes can fuse homotypically [12, 13], thereby sharing ligands within the endosomal network [5, 14]. The transfer of cargo from early to late endosomes occurs either by conversion of Rab5-positive early endosomes into Rab7-positive late endosomes [5, 15, 16] or by budding of carrier vesicles from early endosomes and subsequent fusion with late endosomes [17, 18].

The dynamics of endocytosis and subsequent cargo sorting and transport along the endocytic pathway have been intensively studied in the past, both experimentally and theoretically [6]. By tracking individual endosomes as well as endosomal populations, it was shown that endocytic cargo (LDL) progressively flows from small endosomes at the cell periphery to large endosomes at the center, which eventually convert into late endosomes leading to cargo degradation [5]. Experimental support to such spatiotemporal progression, to which we refer here as the funnel model, has come from a recent genomic survey [19]. Although the discrete structure of the endosomal network is important to understand cargo sorting and flux, theoretical approaches have so far typically focused on the kinetics of integral ligand uptake into endosomal compartments, (e.g., early or late endosomes), without resolving the role of individual endosomes [20–27]. Such approaches ignored the discrete nature of the endosomal network consisting of many individual endosomes distributed in space and evolving in time. This averaging dramatically reduces the information that can be extracted from the experimental data and, consequently, diminishes the ability to resolve the (e.g., kinetic) parameters of the process.

To understand the dynamic organization of the endosomal network, we need to consider the interactions of distinct endosomes undergoing fusion, fission, and conversion. The behavior of the network and its robust operation emerge from the collective behavior of hundreds of individual endosomes.

<sup>6</sup>These authors contributed equally to this work

\*Correspondence: [julicher@pks.mpg.de](mailto:julicher@pks.mpg.de)

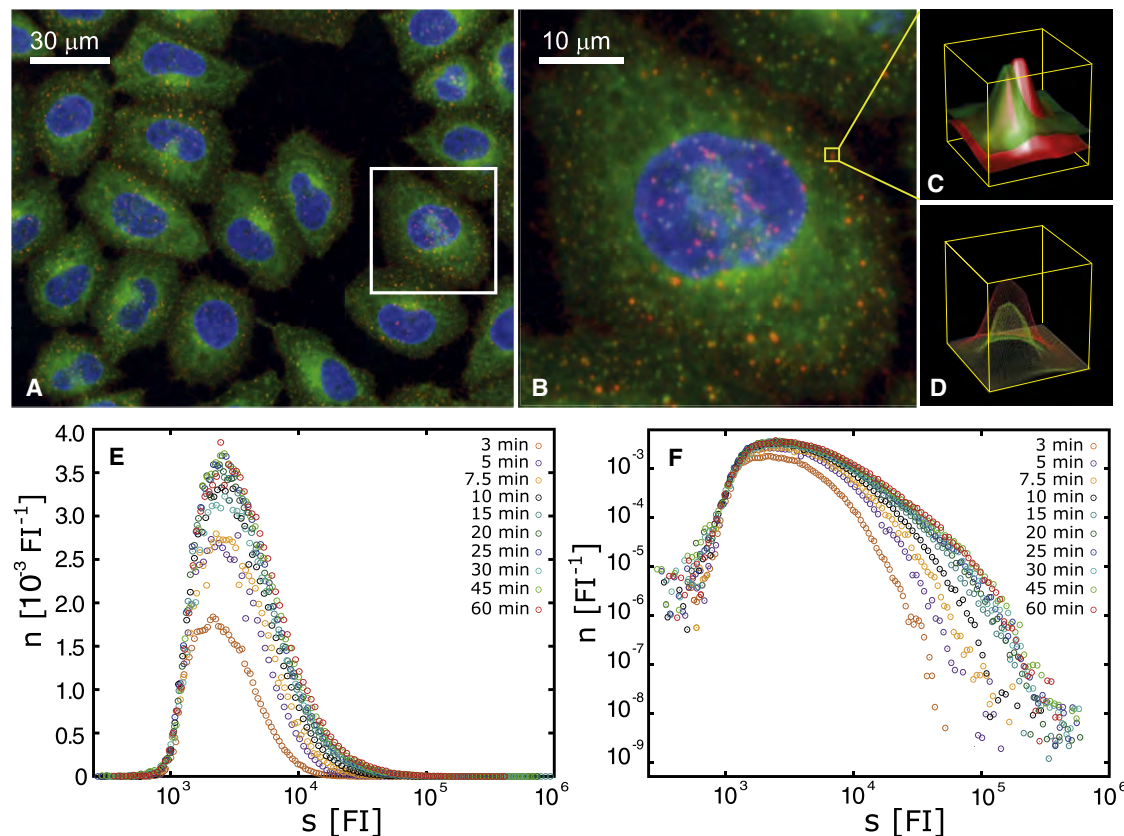


**Figure 1. Quantitative Analysis of Confocal Microscopy Images of HeLa Cells Expressing GFP-Rab5 and Internalizing LDL**

(A) Representative image of HeLa GFP-Rab5c BAC cells after 60 min of continuous uptake of LDL at 37°C in serum-free medium. Before the experiment, cells were grown in full medium to 60%–70% confluency. GFP-Rab5c (green) is expressed under control of the endogenous Rab5 promoter; human LDL (red) is labeled by an antibody against apo-B; nuclei (blue) are labeled by DAPI (see also Figure S1). (B) Higher magnification of a single cell. High-resolution images allow for the identification of individual endosomes. Statistical analysis was carried out for endosomes containing both GFP-Rab5c (green) and LDL (red). (C and D) Vesicle fitting of an individual endosome by motion-tracking image analysis software [5]. The GFP-Rab5c (green) and LDL (red) raw fluorescence intensity profile (C) are used to fit a model function (D) from which vesicle parameters (x-y coordinates, integral intensity, area) are quantified. (E and F) The number  $n(s)\Delta s$  of Rab5-positive endosomes with total LDL intensity in between  $s$  and  $s + \Delta s$  is quantified from image analysis at different times after addition of LDL. The number density  $n(s)$  at different times is plotted in log-linear scale (E) and log-log scale (F). Each data point is the average of three experiments.

The macroscopic kinetic behavior of the endosomal network exhibits properties that are not found in individual endosomes but originate from the collective interplay of many endosomes in a self-organization process [28, 29].

In this study, we present a general theoretical framework to describe the dynamic properties of endosomal networks that takes into account several key microscopic interaction processes and is based on cargo distributions in the endosomal populations. Our approach makes it possible for the first time to determine with high reliability endocytic transport rates that are essentially inaccessible to conventional approaches.

## Results

### Quantitative Image Analysis of the Endosomal Network

In order to study the flux of cargo through the early endosomal network, we used a cell-based, quantitative, high resolution imaging approach. We focused on the uptake and intracellular transport of fluorescently labeled LDL as endocytic marker for the degradative pathway. As cell model system, we used HeLa cells transfected with a bacterial artificial chromosome (BAC) transgene stably expressing GFP-Rab5c under its

endogenous promoter [30] to avoid alterations of the endocytic system due to overexpression (see Figure S1 available online). We imaged cells with high resolution using an automated confocal microscope to resolve individual endosomes as well as image statistically significant endosomal populations. Quantitative multiparametric image analysis (QMPIA) [19] was applied to extract morphometric parameters of the imaged fluorescent structures.

To progressively fill the endocytic system, we allowed cells to internalize LDL at different concentrations (0.5–10  $\mu\text{g/ml}$ ) continuously for different time intervals, fixed and processed for image acquisition. By high-throughput automated microscopy,  $\sim 1,700$  cells were imaged on average at each time point (Figures 1A and 1B). Early endosomes were identified as vesicular structures positive for Rab5 and LDL (Figures 1C and 1D). The number of endosomes containing LDL in each image ( $\sim 20$  cells) ranged from 48 (after 1 min of LDL uptake) to 490 (60 min LDL uptake). For each endosome, we quantified the total LDL fluorescence intensity, denoted  $s$ .

At each time point, the distribution of cargo in the entire network of Rab5-positive endosomes can be characterized by the density  $n(s)$  of endosomes per cell with LDL fluorescence

**Quantitative Study of Endosomal Network Dynamics**

3

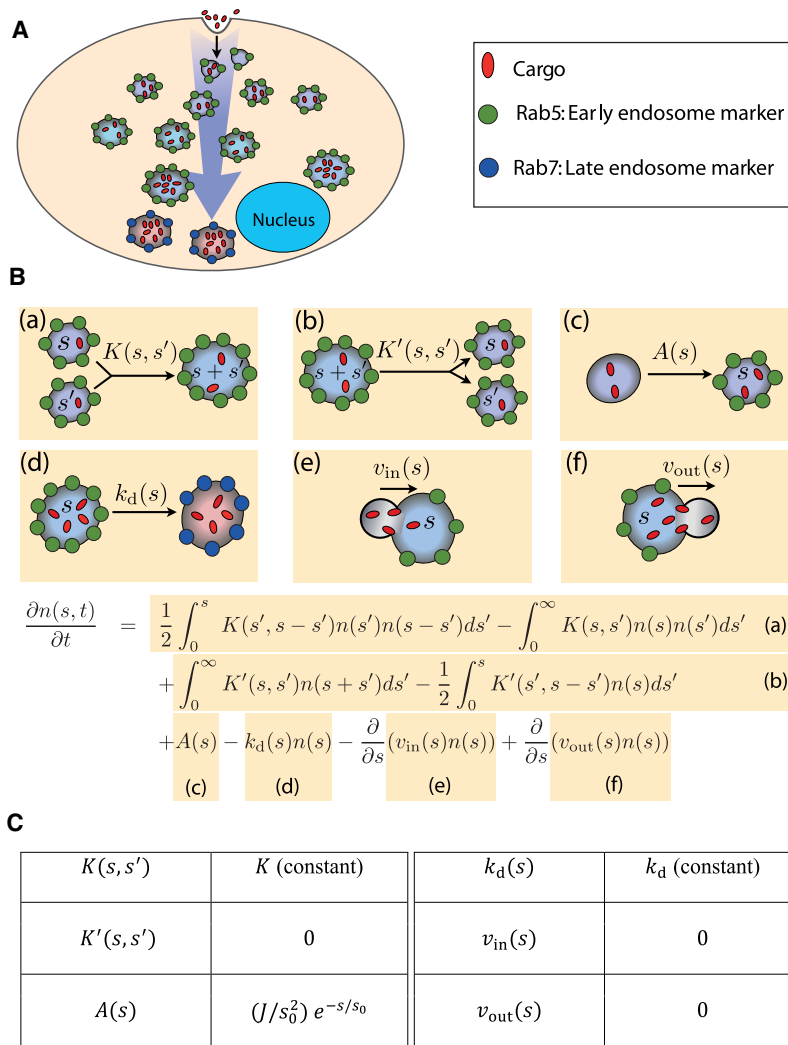


**Figure 2. Theoretical Description of Endosome Network Dynamics**

(A) Schematic representation of endosomal trafficking. Degradative cargo enters via endocytosis and is distributed into a network of early Rab5-positive endosomes. It is finally transferred to late Rab7-positive endosomes and lysosomes.

(B) The schemes (a–f) represent the different processes that govern the distribution of cargo in the early endosomes. The state of the endosomal network is described by the number  $n(s, t)ds$  of endosomal objects per cell, carrying the cargo amount in the interval between  $s$  and  $s + ds$  at time  $t$ . The cargo distribution  $n(s, t)$  obeys a general dynamic equation that accounts for the processes (a–f). (a) Homotypic fusion of two endosomes carrying the cargo amounts  $s$  and  $s'$  leads to the replacement of the two endosomes by a new one carrying the LDL amount  $s + s'$ . Such fusion occurs at the rate  $K(s, s')$ . (b) Two endosomes carrying the cargo amounts  $s$  and  $s'$  can be produced by the fission of endosomes carrying the cargo amount  $s + s'$ . Such fission occurs at the rate  $K'(s, s')$ . (c) As cargo flows, new endosomes carrying the amount  $s$  of cargo appear at the rate  $A(s)$ . (d) Early endosomes disappear from the system by undergoing conversion to late endosomes at the rate  $k_d(s)$ . Finally, endosomes can take up additional cargo by fusing with endocytic vesicles (e) and can lose cargo by budding off vesicular structures (f) [17, 18]. The currents  $v_{in}(s)$  and  $v_{out}(s)$  are the average cargo amount per unit of time respectively gained and lost by an endosome carrying the cargo amount  $s$ . Cargo enters the network via the processes (b) and (e). The total cargo influx is  $J = \int_0^\infty (sA(s) + v_{in}(s)n(s))ds$ .

(C) Choice of parameters defining the Entry-Fusion-Exit model.

sensitivity of the light microscopy, the number of endosomes with small amounts of LDL is underestimated.

**Theoretical Description of Endosomal Dynamics**

In order to understand the time-dependence of  $n(s)$ , we formulated a general theoretical description of endosomal dynamics, which is based on the idea that cargo distribution evolves over time as a result of endosome fusion and fission in addition to the in-flux and out-flux of cargo, see Figure 2A. If two endosomes fuse homotypically, they form a new endosome, which carries the combined cargo of the original ones (Figure 2B, a). If an endosome undergoes homotypic fission, the cargo is redistributed into two newly formed endosomes (Figure 2B, b). The total cargo influx into the early endosomal network denoted by  $J$  could occur by the heterotypic fusion of cargo-carrying endocytic CCV with Rab5-positive and cargo-carrying early endosomes (Figure 2B, e). Alternatively, cargo-loaded Rab5-positive endosomes may appear either by conversion or coalescence of CCV or by their fusion with a pre-existing endosome devoid of cargo (Figure 2B, c). Finally, cargo can leave the early endosomal network either when cargo-carrying Rab5-positive early endosomes are converted into Rab7-positive late endosomes (Figure 2B, d) or via the heterotypic fission of cargo-carrying Rab5-positive endosomes (Figure 2B, f). The evolution of the network over time is described by a general kinetic equation for the cargo distribution  $n(s)$ , which accounts for all the key processes governing the network (see Figure 2B). The parameters that enter such equation are the rates at which each process occurs. The equation of Figure 2B is a generalization of the Smoluchowski

intensity  $s$ . More precisely,  $n(s)\Delta s$  is the number of Rab5-positive endosomes per cell for which the LDL fluorescence intensity is in the interval between  $s$  and  $s + \Delta s$  (see [Supplemental Experimental Procedures](#)). Fluorescence intensity (FI) is measured in arbitrary units. The total number of cargo-carrying Rab5-positive endosomes per cell is  $N = \int_0^\infty n(s)ds$  and the total LDL fluorescence in the endosomes is  $\Phi = \int_0^\infty sn(s)ds$ . In the course of cargo uptake, the change over time of  $n(s)$  reflects the collective endosome dynamics. Figure 1 shows the experimentally measured cargo distributions  $n(s)$  at different times after addition of 2.5  $\mu\text{g/ml}$  LDL in semi-logarithmic (Figure 1E) and double-logarithmic scales (Figure 1F) to better visualize the differences of distributions over the wide range of cargo intensity and number of structures. At early times, the distribution  $n(s)$  is narrow and peaked at a small intensity value whose amplitude increases with time, showing that LDL initially enters many endosomes in small quantities (Figure 1E). Subsequently the distribution  $n(s)$  broadens, showing that LDL concentrates at higher amounts in an increasing number of endosomes (Figure 1F). After about 30 min, the distribution  $n(s)$  has reached steady state. Here, the distribution of cargo amounts in individual endosomes has a broad tail and ranges over three orders of magnitude of fluorescence intensity (Figure 1F). Note that, due to the limited

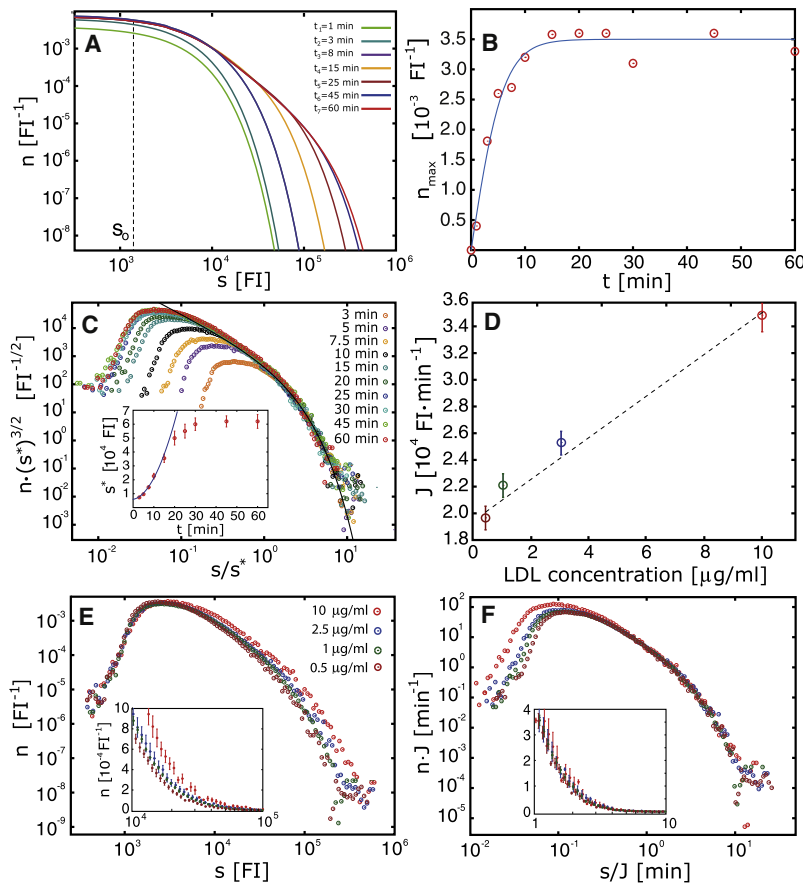


**Figure 3. Testing the Theoretical Predictions of the Entry-Fusion-Exit Model**

(A) Numerical solution of the kinetic equation (Figure 2B) in the EFE model (Figure 2C) at different times 3–60 min after allowing the internalization of the cargo into the endosomal network. At the initial time  $t = 0$ , the system does not contain cargo  $n(s, t = 0) = 0$ . Here we set  $J/K = 1.8 \cdot 10^6$  FI,  $s_0 = 1885$  FI,  $k_d/K = 2.9$  (see also Figure S2).

(B) The maximum  $n_{\max}$  of the experimental distributions  $n(s)$ , shown in Figure 1, at different times (red circles). The solid blue line represents the fit of the function  $n_{\max}(s, t) = C \tanh(t / \tau)$  to the data, where we obtain from the fit  $C = 3.48 \cdot 10^{-3}$  FI $^{-1}$  and  $\tau = 7$  min.

(C) Experimental distributions  $n(s)$  at different times, shown in Figure 1, plotted on rescaled axes. The x axis is  $s/s^*$  and y axis is  $n(s, t) \cdot s^{3/2}$ , where  $s^*$  is a time-dependent scaling factor such that the rescaled distributions collapse on the line  $n_0(s/s^*)^{-3/2} e^{-s/s^*}$  (shown in black) with  $n_0 = 1.4 \cdot 10^3$  FI $^{-1}$ . The inset shows  $s^*$  at different times (red circles). At early times,  $s^*(t)$  is well fit to a  $t^2$  function (blue curve).

(D) LDL influx  $J$  in Rab5-endosomes for different LDL concentrations.  $J$  is obtained from the fit of Equation 5 to the experimental data of the total LDL fluorescence intensity in Rab5-endosomes  $\Phi(t)$  shown in Figure 5C. Error bars represent the SE obtained in the fit procedure.

(E) Experimental distribution  $n(s)$  after 45 min internalization of LDL for four different LDL concentrations. Error bars represent the SD calculated from three experiments.

(F) Same distributions rescaled by the LDL influx  $J$  reveals the data collapse as predicted by the theory. The insets in (E) and (F) show the same collapse in semi-log scale.

coagulation equation [31]. Similar equations have been studied in a variety of other problems [32–36].

### Entry-Fusion-Exit Model

The main features of the experimentally observed LDL distributions can be captured by three main processes: source of cargo-carrying early endosomes, homotypic early endosome fusion, and early-to-late endosome conversion. With the simplified choice of (1) a constant fusion rate  $K$ , (2) a constant conversion rate  $k_d$ , and (3) a source of cargo-loaded endosomes described by a source function  $A(s) = (J/s_0^2) e^{-s/s_0}$  (see Figure 2B), where  $s_0$  is a typical cargo amount in newly appearing endosomes, we can analytically solve the equation of Figure 2B (see Theoretical Methods in Supplemental Information). Note that our main results do not depend on the specific choice of the function  $A(s)$ , as long as it decays rapidly with  $s$ . The results only depend on the scale over which  $A(s)$  decays and on the cargo influx  $J = \int_0^\infty A(s) s ds$  (see Theoretical Methods in Supplemental Information). The shape of calculated cargo distribution  $n(s)$  at different time points obtained by the numerical solution of the dynamic equation using these parameters and ignoring endosome fission ( $K' = 0$ ) and other cargo exchange processes ( $v_{\text{in}} = 0$  and  $v_{\text{out}} = 0$ ) is shown in Figure 3A. We call the scenario described by this set of parameters the Entry-Fusion-Exit (EFE) model (see Figure 2C). At early times, the cargo distribution  $n(s)$  is narrow and peaked around  $s_0$  with maximal value  $n_{\max}$ . This maximal value increases with time and saturates after a characteristic time  $\tau = (JK/(2s_0))^{-1/2}$ , which depends on the rate of homotypic endosome fusion  $K$  and on the influx  $J$ .

Subsequently, endosome fusion leads to broadening of the distribution, which covers an increasingly large range of cargo amount  $s$  in which the distribution follows a power-law decay  $n(s) \sim s^{-3/2}$ . After a characteristic time, which is determined by  $k_d^{-1}$ , the distribution reaches a steady state profile with

$$n(s) = \left( \frac{J}{2\pi K} \right)^{1/2} \frac{e^{-s/s_\infty}^2}{s^{3/2}} \quad (1)$$

for  $s > s_0$ . This profile is characterized by a power-law followed by an exponential tail for  $s > s_\infty^*$ , where  $s_\infty^* = 2JK/k_d^2$ . While the cargo distribution  $n(s)$  is broadening, the power-law emerges by gradually shifting the exponential tail toward increasing values of  $s$ . For  $s$  larger than  $s_0$ , the time-dependent distribution is well described by  $n(s, t) \equiv (J/(2\pi K))^{1/2} s^{-3/2} \exp(-s/s^*(t))$  where only  $s^*(t)$  is time dependent. For short times, the EFE model predicts  $s^*(t) \equiv JKt^2$ . After long times,  $s^*(t)$  reaches the steady state value  $s_\infty^*$ . For details, see the Theoretical Methods in Supplemental Information.

### Comparison of the Model Predictions with the Experimental Data

We tested the predictions of this model by comparison with the experimental results. The experimental data exhibit all key features predicted by our EFE model. Time evolution of the maximum value  $n_{\max}$  of the cargo distribution  $n(s)$  follows the theoretical prediction (see Figure 3B; Supplemental Information). For an LDL concentration of 2.5  $\mu\text{g/ml}$ , the characteristic time for the amplitude of the distribution to reach steady state is about  $\tau = 7 \pm 0.5$  min (see Figure 3B). The

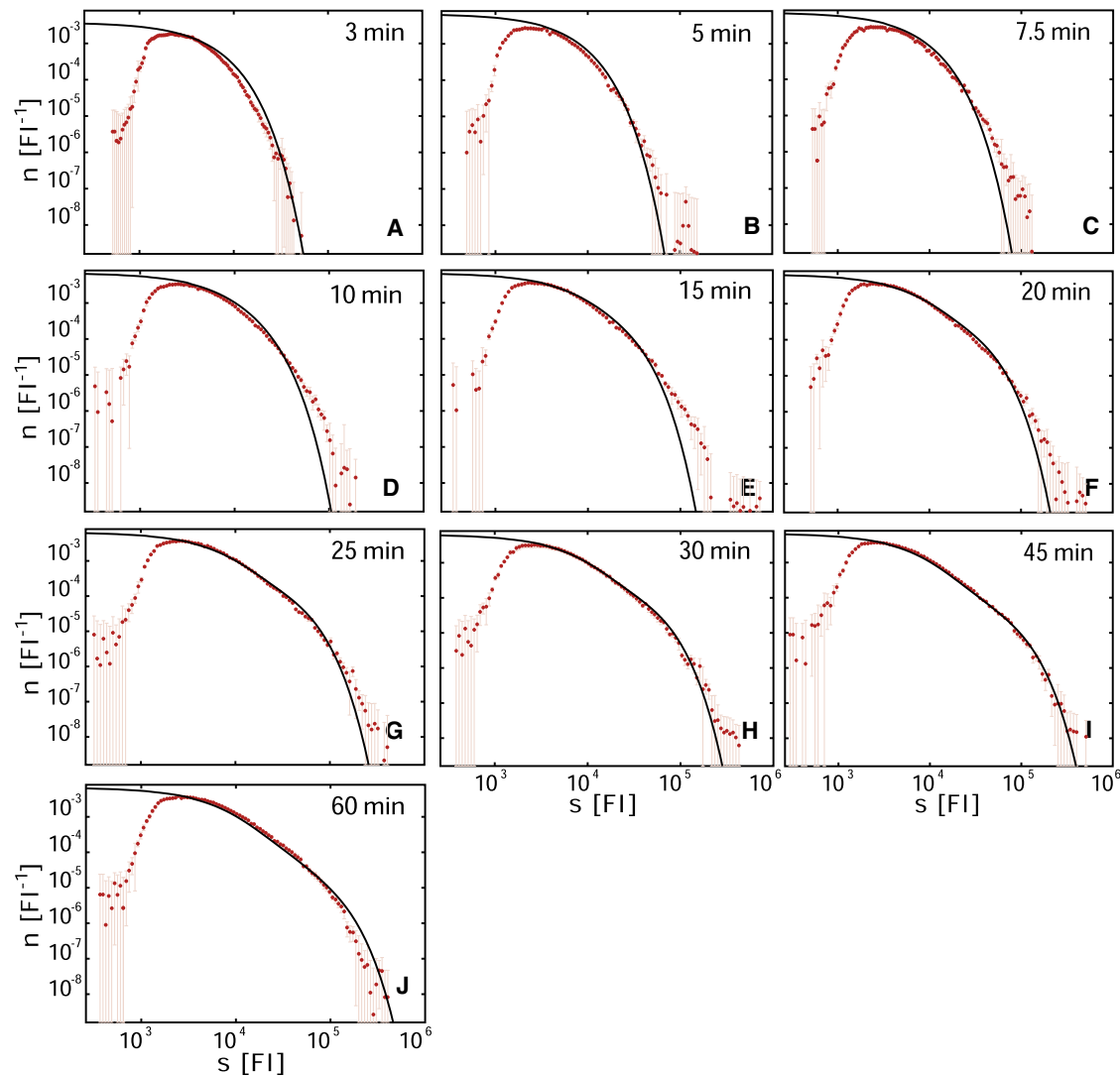


Figure 4. Time Course of LDL Distribution in Rab5 Endosomes—Theory Compared to Experiments

(A–J) Fit of the Entry-Fusion-Exit model to the experimental LDL distributions (red circles) at different times after addition of LDL. The purple solid lines are the numerical solutions of the kinetic equation (Figure 2B) with the parameters choice and value reported in Figure 2C and Table 1 (second column), respectively.

theoretical prediction that the shape of the distribution for  $s > s_0$  only depends on time via  $s^*$  can be tested by plotting the experimental data as  $n(s) \cdot (s^*)^{3/2}$  versus  $s/s^*$  (see Figure 3C). This figure shows that the data at different times collapse on the same functional form (black line) as predicted. The time dependence of  $s^*$  is shown in the inset of Figure 3C. As predicted by the theory, it increases with time as  $t^2$  (blue line) at early times and saturates at later times.

We further tested the accuracy of the EFE model by studying the influence of the LDL influx  $J$  on the shape of the cargo distribution  $n(s)$  at a given time. The model predicts that the distribution amplitude increases proportionally to the square root of  $J$ ,  $n(s) \sim J^{1/2}$  and that at any time point,  $s^* \sim J$  (see Theoretical Methods in Supplemental Information). Our experimental data allow us to test these predictions. The LDL influx  $J$  depends on the concentration of labeled cargo (see Figure 3D and below). We estimated  $J$  for the different concentrations of LDL from the time evolution of the total LDL fluorescence intensity  $\Phi(t)$  (see Figure 5C as well as Equations 4 and 5).

The observed distributions at 45 min differ for different cargo concentrations (see Figure 3E). The experimental data follows the predictions of our model. This is shown in Figure 3F where the data of Figure 3E collapses on a single curve when plotted on axes that are rescaled by the LDL influx according to the predicted scaling. The same collapse can also be seen in semi-log representation (see Figure 3F inset). This square root dependence of the distribution amplitude on the influx is striking and a direct consequence of fusion events. This observation provides strong support for a scenario in which cargo transport is dominated by fusion processes with a constant fusion kernel  $K$ .

Our simplified model can account quantitatively for the full shapes of observed cargo distributions  $n(s)$  as a function of time (see Figure 4). Here, the solid lines indicate fits of numerical solutions to the dynamic equation for  $n(s)$  to the experimental data. These fits are obtained for the EFE model with parameters given in Table 1. From this fit, the values of all kinetic parameters are obtained. For details of the fitting

Table 1. Estimate of Kinetic Rates

Parameters of EFE model	Parameter values	EEA1 knockdown (change relative to Control)
$K$ (constant)	$K = 1.6 \cdot 10^{-4} \text{ s}^{-1}$	$K = -38.3\%$
$(J/s_0^2)e^{-s/s_0}$	$J = 546 \text{ FI} \cdot \text{s}^{-1}, s_0 = 3600 \text{ FI}$	$J = -58.2\%, s_0 = +13.7\%$
$k_d$ (constant)	$k_d = 1.5 \cdot 10^{-3} \text{ s}^{-1}$	$k_d = -40\%$

The left column lists the parameter choice of the EFE model. The middle column presents the corresponding values of the kinetic rates obtained from the fit of the EFE model to the experimental time course of LDL distribution, Figure 4. The right-most column presents the relative change in the magnitude of kinetic parameters after EEA 1 knockdown as compared to the control experiments.

procedure, see Numerical Methods in [Supplemental Information](#). For an LDL concentration of 2.5  $\mu\text{g/ml}$ , we find  $K = 1.6 \cdot 10^{-4} \text{ s}^{-1}$ ,  $s_0 = 3600 \text{ FI}$ ,  $k_d = 1.5 \cdot 10^{-3} \text{ s}^{-1}$ , and  $J = 546 \text{ FI} \cdot \text{s}^{-1}$ . These values imply that  $\sim 9$  new endosomes with typical cargo amount of  $s_0 = 3,600 \text{ FI}$  appear per cell per min. At steady state, the average time between two fusion events for a cargo-carrying endosome is about  $1/KN_0 \cong 3 \text{ min}$ . Here,  $N_0 = 32$  is the total number of Rab5-positive early endosomes containing internalized LDL per cell confocal section at steady state. Finally, the conversion rate is found to be  $k_d^{-1} \cong 11 \text{ min}$ . We also tested the influence of two additional processes by performing fits of the data to an expanded EFE model with constant fission  $K'$  and constant  $v_{\text{out}}$ . This analysis leads to an estimate for the ratio between frequencies of fission and fusion events  $2K'/KN_0 = 0.26$  and for the cargo flux  $v_{\text{out}}$ , which is less than 5% of the conversion flux. From this analysis, we conclude that the influx  $J$ , fusion with a constant rate  $K$ , and constant conversion rate  $k_d$  determine the main features of the LDL distributions in the early endocytic network. Other processes such as homotypic and heterotypic fission of endosomes occur but do not play a dominant role to shape the LDL distribution. The experiments also obey the theoretical predictions for the total number of LDL-carrying endosomes  $N(t)$  and for the total LDL intensity  $\Phi(t)$ . The time dependence of the number of cargo-carrying endosomes  $N(t)$  and of the total LDL fluorescence  $\Phi(t)$  of the endosomes after initiating cargo uptake at  $t = 0$  are displayed in [Figures 5A](#) and [5C](#) for four different LDL concentrations. Interestingly, the functional forms of  $N(t)$  and  $\Phi(t)$  are different. The endosome number  $N$  reaches a plateau value earlier than the total fluorescence intensity  $\Phi$ . Our theory allows explaining such difference.

In the EFE model, the total number of cargo-carrying endosomes  $N(t)$  obeys:

$$\frac{dN}{dt} = -\frac{KN^2}{2} - k_d N + \frac{J}{s_0} \quad (2)$$

If endosome loss by fusion out-numbers endosome conversion,  $\tau \ll 1/k_d$  where  $\tau = (2s_0/(JK))^{1/2}$ , the solution of [Equation 2](#) is

$$N(t) \cong N_0 \tanh\left(\frac{t}{\tau}\right), \quad (3)$$

where  $N_0 = (2J/(Ks_0))^{1/2}$  is the steady state number of cargo-carrying endosomes.  $N$  reaches the steady-state value after the characteristic time  $\tau$ . Note that  $\tau$  is also the typical time after which the distribution maximum,  $n_{\text{max}}$  saturates (see [Figure 3B](#)). The observed time dependence of the total number of cargo-carrying endosomes is indeed well described by the function given in [Equation 3](#) (see [Figure 5A](#)). In addition,

[Equation 3](#) predicts that the observed functions  $N(t)$  should collapse on the same curve provided that the total endosome number  $N$  and the time  $t$  are appropriately rescaled by the LDL influx  $J$ . This is indeed the case (see [Figure 5B](#)).

Furthermore,  $\Phi(t)$  obeys

$$\frac{d\Phi}{dt} = J - k_d \Phi. \quad (4)$$

The solution is

$$\Phi(t) = \left(\frac{J}{k_d}\right) (1 - e^{-k_d t}). \quad (5)$$

The theory predicts that total intensity  $\Phi$  relaxes exponentially during a time  $k_d^{-1}$  to a steady state value  $J/k_d$ . The observed behavior of total LDL intensity shown in [Figure 5C](#) is well fit by the function given in [Equation 5](#). We used this fit to obtain the influx  $J$  and the conversion rate  $k_d$  for the different LDL concentrations. We find that the LDL influx  $J$  increases with the concentration of LDL in the culture medium but the exit rate is nearly constant ([Figures 5D](#) and [6D](#)).

We have identified two different time scales governing the dynamics of LDL-positive endosomes. The fast relaxation of endosome number  $N$  and of the distribution amplitude occurs in a characteristic time  $\tau$ , which depends on the kinetics of homotypic fusion and appearance of LDL-loaded endosome. In addition, there is a comparatively slow saturation of total cargo amount  $\phi$  and of  $s^*$  (characterizing the broadness of cargo distribution) that occurs after a characteristic time  $k_d^{-1}$ , which is governed by cargo exit from the network.

The dynamic equation for the cargo distribution shown in [Figure 2B](#) allows for fusion and conversion rates to be cargo-dependent. We therefore studied the effects of such cargo dependence on the resulting distributions  $n(s,t)$ . A detailed analysis provided in the [Supplemental Information](#) suggests that the fusion rate  $K(s, s')$  is a constant, independent of cargo amounts  $s$  and  $s'$  of the fusing endosomes. This implies that LDL behaves as a neutral cargo that does not influence the endosomal fusion rate. Second, conversion is the major mechanism for LDL exiting the early endosome compartment. The experimental data are best described using a conversion rate  $k_d$ , which is again independent of cargo amount (Theoretical Methods in [Supplemental Information](#)). Furthermore, our analysis reveals that the source function  $A(s)$  must decay rapidly for  $s > s_0$ , reflecting the observation that newly appearing early endosomes typically contain small amount of cargo  $s_0$ . Note that the detailed shape of  $A(s)$  has only influence on the shape of  $n(s)$  for small  $s \leq s_0$  (see Theoretical Methods in [Supplemental Information](#)).

### Changes of the Kinetic Parameters in a Perturbation Experiment

Our approach can be used to infer changes of kinetic parameters of the endocytic system under perturbed conditions, thereby testing predictions about the effects of perturbations on endosome kinetics and interactions. To demonstrate this point, we reduced the levels of the Rab5 effector and endosomal tethering factor EEA1 [37] by RNAi (see Experimental Procedures). Depletion of EEA1 is expected to inhibit the fusion of CCV with early endosomes [38] and thus cargo entry  $J$ , as well as homotypic early endosome fusion [39]. Because endosome fusion is required for cargo progression from early to late endosomes [5], it would be expected to slow down also endosome conversion. HeLa cells were transfected with small

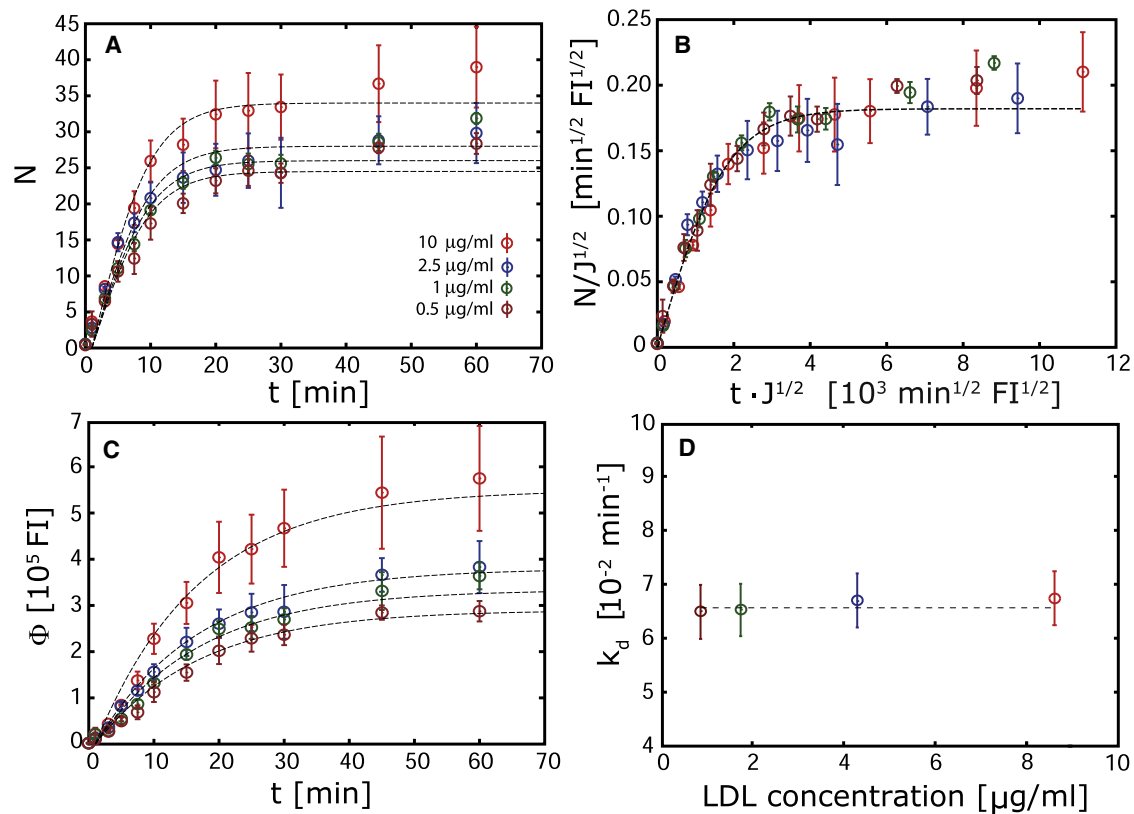


Figure 5. Time Course of the Number of LDL-Carrying Endosomes and of the Total LDL Amount in the Population of Rab5-Positive Early Endosomes  
 (A) Experimental data of the total number of LDL-carrying Rab5-endosomes  $N(t)$  at different times after addition of LDL for four different concentrations of LDL. The dashed lines represent the fit of the function given in Equation 3 to the experimental data. Error bars represent the SD calculated from three experiments.  
 (B) Number of cargo-positive Rab5-endosomes as a function of time  $N(t)$  shown in Figure 5A rescaled by  $J^{1/2}$ . The dashed line represents the theoretical prediction; see Equation 3.  
 (C) Experimental data of the total LDL fluorescence intensity in Rab5-endosomes  $\Phi(t)$  at different times after addition of LDL for four different concentrations of LDL. The dashed lines represent the fit of the functions given in Equation 5 to the data. Error bars represent the SD calculated from three experiments.  
 (D) Rate of LDL exit from the network of Rab5-endosomes  $k_d$ , for four different LDL concentrations obtained from the fit of the function given by Equation 5 to the total LDL fluorescence intensity in Rab5 endosomes  $\Phi(t)$  shown in (C). Error bars represent the SE calculated in the fit procedure.

interfering RNAs against EEA1 72 hr prior to LDL internalization. The distribution  $n(s)$  was quantified at different times in a LDL step-chase experiment, both for EEA1 knockdown and control cells (Figures 6A–6F; Figures S3 and S4). By performing fits of the EFE model to the experimental data, we determined the values of the influx  $J$ , fusion  $K$ , and conversion rates  $k_d$  for the EEA1 RNAi and control conditions (see Figures 6A–6F; Supplemental Information). Our analysis indeed revealed a significant decrease in the rate of  $J$ ,  $K$ , and a moderate slow-down of  $k_d$  upon EEA1 depletion (Figures 6G–6I; Table 1), in line with the predictions from previous biological knowledge. This experiment validates our approach, demonstrating that it can detect effects of weak perturbations with high sensitivity.

## Discussion

In this study, we developed a theoretical framework to describe how the structure and large-scale properties of the endosomal network emerge from the collective behavior of many endosomes. This theory is based on elementary processes of the endosomal network (Figure 2). We tested it by experimental studies of endosomal populations in which LDL-carrying early

endosomes were analyzed using cell imaging and QMPIA. Our systems analysis led to four important conclusions. First, despite the multiplicity of regulatory steps and trafficking mechanisms (Figure 2), the main features of LDL transport through the endosomal network and its trafficking dynamics can be understood with very few simple rules, where homotypic endosome fusion plays a key role. Second, the combination of theory and experiments supports the funnel model of endosome progression [5, 19]. Third, our approach allows measuring kinetic transport rates, which are normally difficult to determine experimentally, from a series of still images. Finally, our results suggest that Rab conversion [5, 19] instead of vesicle budding is the principal mode of transport of LDL from early to late endosomes.

Our theoretical framework predicts specific scaling properties of cargo distributions, which we confirmed in experiments in which endosomal parameters such as the number of endosomes and their cargo content were measured quantitatively. Furthermore, we have shown that the whole time course of cargo distribution in the endosomal network can be quantitatively accounted for by our theory. Our approach differs from traditional studies based on biochemical assays measuring average concentrations and fluxes in the cell and associated

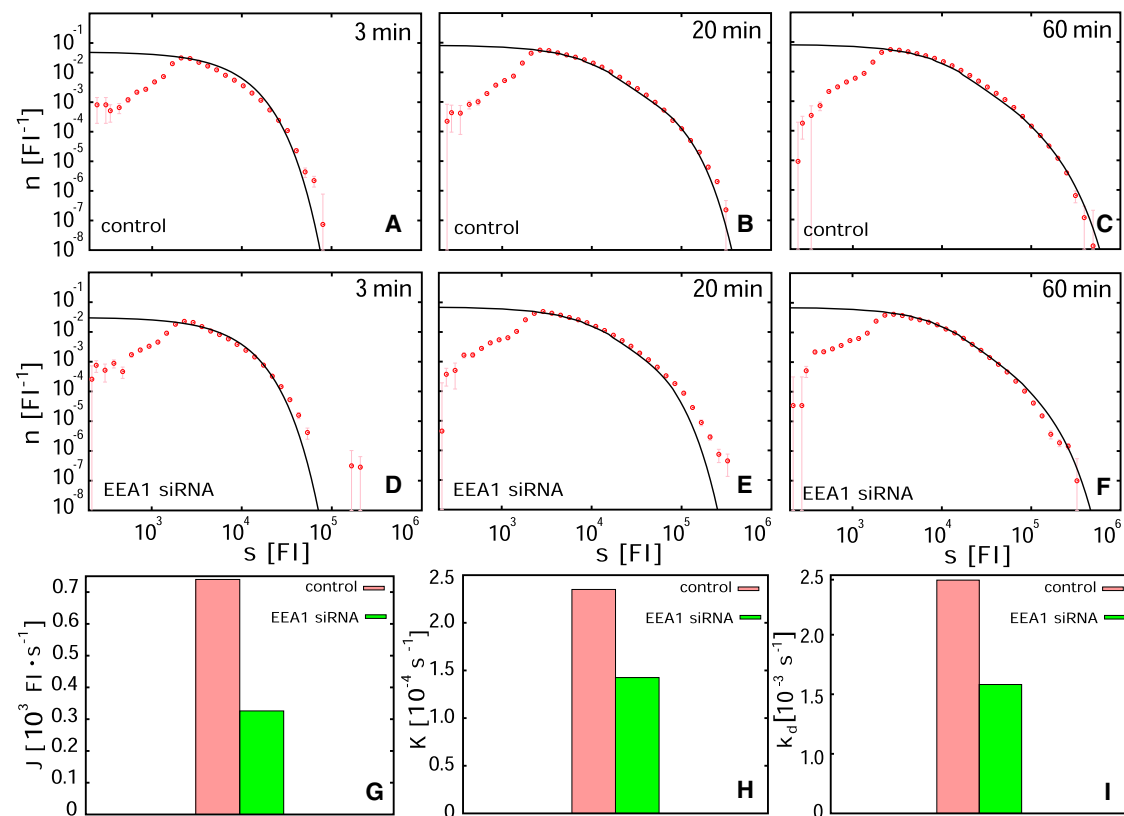


**Figure 6. Perturbation of Endosome Dynamics in an EEA1 Knockdown Experiment**

(A–C) Cargo distribution  $n(s)$  (red circles), obtained for cells under control conditions, at three different times after addition of LDL. The fits of the EFE model (Figures 2B and 2C) are shown (solid black lines), see also Figure S3. Error bars represent the SD calculated from three experiments.

(D–F) Cargo distribution  $n(s)$  (red circles), obtained for EEA1-depleted cells, at three different times after addition of LDL. The fits of the EFE model (Figures 2B and 2C) are shown (solid black lines), see also Figure S4. Error bars represent the SD calculated from three experiments.

(G–I) Values of the kinetic parameters  $J$ ,  $K$ ,  $k_d$ , obtained from the fit to the time-course of  $n(s)$  for control (red) and EEA1 knockdown experiments (green) (Table S1; Supplemental Information).

kinetic rates. Using imaging, we could exploit information of the distribution of cargo in distinct endosomes. The large number of endosomes observed allowed us to obtain statistically significant data about the properties of the tails of cargo distributions, which carry interesting information about the endosomal network dynamics.

From our analysis, we deduced that three main processes govern LDL trafficking and dynamics through the endosomal network: A source of cargo-carrying early endosomes (cargo entry), homotypic early endosome fusion (cargo concentration), and exit of cargo from the early endosomal network via endosome conversion (for cargo degradation). The funnel model, which is based on endosome tracking in living cells and functional genomics studies [5, 19], characterizes the endosomal system as a continuously evolving population of endosomes that progressively grow in size and move from the cell periphery to the center as they concentrate cargo for degradation and prepare for conversion. An important result of our work is that homotypic endosome fusion plays a key role in shaping the network. This probably reflects the need to progressively accumulate LDL from many small into few large endosomes for degradation [5]. The situation might be different for transferrin, which recycles to the cell surface. In this case, endosome fission is expected to play a more important role than for LDL.

It has been postulated that cargo induces the assembly of the endocytic transport machinery thereby determining the kinetic properties of the endosomal network [25]. Our parameter estimates show that the fusion kernel is constant to a good approximation and that fusion does not depend on LDL levels. This implies that the endosomal system functions largely independently of the presence of LDL. Evidently, the endocytic pathway operates to a certain extent autonomously, i.e., supporting membrane turnover irrespective of the influx of endocytic cargo. However, other types of cargo such as signaling molecules (e.g., EGF) are known to exert a pronounced influence on the behavior of the endocytic network [5, 19].

Previous studies have shown that transfer of cargo from early to late endosomes can occur via two nonexclusive mechanisms. Whereas viral cargo exits from early endosomes harboring Rab5 by the budding of Rab7-positive vesicles [17, 18], LDL-containing endosomes undergo conversion from a Rab5 to a Rab7 compartment [5]. The fact that the Entry-Fusion-Exit model can account for all key features of the experimental data in different experimental conditions suggests that endosome conversion is the predominant mechanism for the cargo (LDL) and cellular (HeLa) model systems analyzed here. Cargo other than LDL may follow different rules. LDL-harboring endosome fission and cargo exchange

processes play a minor role for overall network shape and dynamics. An estimate of the kinetic rates of these subdominant processes will thus require further experimental data and analysis.

Our approach demonstrated to be sensitive to weak perturbations and capable of quantifying changes of kinetic parameters. By testing predictions about the effects of EEA1 silencing on the network properties, we could show the potential of our theoretical framework as a general tool for the quantitative analysis of intracellular transport between compartments.

Because cargo distribution can vary in response to changes of the endocytic system, our analysis provides a powerful tool for the study of genetic and chemical perturbations that may alter specific systems properties. For example, this could allow understanding the function of specific genes that regulate endosome fusion and fission by analyzing alterations of cargo distributions under gene knockdown conditions. Finally, our population analysis of endosomal networks could be applied to other endosome markers, types of cargo, vesicular structures in the cell, and in more physiological systems such as tissues and organs where kinetic properties can normally be inferred only by technically demanding live imaging approaches.

#### Supplemental Information

Supplemental Information includes seven figures, one table, and Supplemental Experimental Procedures and can be found with this article online at <http://dx.doi.org/10.1016/j.cub.2012.06.021>.

#### Acknowledgments

We would like to thank M. Stöter and C. Möbius from the High-Throughput Technology Development Studio at the MPI-CBG for helping in the automated image acquisition. This work was financially supported by the Virtual Liver initiative (<http://www.virtual-liver.de>), funded by the German Federal Ministry of Research and Education (BMBF) and the Max Planck Society (MPG).

Received: October 6, 2011

Revised: April 13, 2012

Accepted: June 7, 2012

Published online: June 28, 2012

#### References

- van der Goot, F.G., and Gruenberg, J. (2006). Intra-endosomal membrane traffic. *Trends Cell Biol.* *16*, 514–521.
- Mellman, I. (1996). Endocytosis and molecular sorting. *Annu. Rev. Cell Dev. Biol.* *12*, 575–625.
- Conner, S.D., and Schmid, S.L. (2003). Regulated portals of entry into the cell. *Nature* *422*, 37–44.
- Maxfield, F.R., and McGraw, T.E. (2004). Endocytic recycling. *Nat. Rev. Mol. Cell Biol.* *5*, 121–132.
- Rink, J., Ghigo, E., Kalaidzidis, Y., and Zerial, M. (2005). Rab conversion as a mechanism of progression from early to late endosomes. *Cell* *122*, 735–749.
- Dunn, K.W., McGraw, T.E., and Maxfield, F.R. (1989). Iterative fractionation of recycling receptors from lysosomally destined ligands in an early sorting endosome. *J. Cell Biol.* *109*, 3303–3314.
- Zerial, M., and McBride, H. (2001). Rab proteins as membrane organizers. *Nat. Rev. Mol. Cell Biol.* *2*, 107–117.
- Grosshans, B.L., Ortiz, D., and Novick, P. (2006). Rabs and their effectors: achieving specificity in membrane traffic. *Proc. Natl. Acad. Sci. USA* *103*, 11821–11827.
- Pfeffer, S., and Aivazian, D. (2004). Targeting Rab GTPases to distinct membrane compartments. *Nat. Rev. Mol. Cell Biol.* *5*, 886–896.
- Stenmark, H. (2009). Rab GTPases as coordinators of vesicle traffic. *Nat. Rev. Mol. Cell Biol.* *10*, 513–525.
- Zeigerer, A., Gilleron, J., Bogorad, R.L., Marsico, G., Nonaka, H., Seifert, S., Epstein-Barash, H., Kuchimanchi, S., Peng, C.G., Ruda, V.M., et al. (2012). Rab5 is necessary for the biogenesis of the endolysosomal system in vivo. *Nature* *485*, 465–470.
- Bucci, C., Parton, R.G., Mather, I.H., Stunnenberg, H., Simons, K., Hoflack, B., and Zerial, M. (1992). The small GTPase rab5 functions as a regulatory factor in the early endocytic pathway. *Cell* *70*, 715–728.
- Gorvel, J.-P., Chavier, P., Zerial, M., and Gruenberg, J. (1991). rab5 controls early endosome fusion in vitro. *Cell* *64*, 915–925.
- Roberts, R.L., Barbieri, M.A., Pryse, K.M., Chua, M., Morisaki, J.H., and Stahl, P.D. (1999). Endosome fusion in living cells overexpressing GFP-rab5. *J. Cell Sci.* *112*, 3667–3675.
- Dunn, K.W., and Maxfield, F.R. (1992). Delivery of ligands from sorting endosomes to late endosomes occurs by maturation of sorting endosomes. *J. Cell Biol.* *117*, 301–310.
- Del Conte-Zerial, P., Bruschi, L., Rink, J.C., Collinet, C., Kalaidzidis, Y., Zerial, M., and Deutsch, A. (2008). Membrane identity and GTPase cascades regulated by toggle and cut-out switches. *Mol. Syst. Biol.* *4*, 206.
- Vonderheit, A., and Helenius, A. (2005). Rab7 associates with early endosomes to mediate sorting and transport of Semliki forest virus to late endosomes. *PLoS Biol.* *3*, e233.
- Murphy, R.F. (1991). Maturation models for endosome and lysosome biogenesis. *Trends Cell Biol.* *1*, 77–82.
- Collinet, C., Stöter, M., Bradshaw, C.R., Samusik, N., Rink, J.C., Kensi, D., Habermann, B., Buchholz, F., Henschel, R., Mueller, M.S., et al. (2010). Systems survey of endocytosis by multiparametric image analysis. *Nature* *464*, 243–249.
- Becker, V., Schilling, M., Bachmann, J., Baumann, U., Raue, A., Maiwald, T., Timmer, J., and Klingmüller, U. (2010). Covering a broad dynamic range: information processing at the erythropoietin receptor. *Science* *328*, 1404–1408.
- Kruse, K., Pantazis, P., Bollenbach, T., Jülicher, F., and González-Gaitán, M. (2004). Dpp gradient formation by dynamin-dependent endocytosis: receptor trafficking and the diffusion model. *Development* *131*, 4843–4856.
- Lauffenburger, D.A., and Lindermann, J.J. (1993). *Receptors: Model for Binding, Trafficking and Signaling* (New York: Oxford University Press).
- Klausner, R., Van Renswoude, J., Harford, J., Wofsy, C., and Goldstein, B. (1985). Mathematical modeling of receptor-mediated endocytosis. In *Endocytosis*, I. Pastan and M.C. Willingham, eds. (New York: Plenum Press), pp. 259–277.
- Tzafiriri, A.R., Wu, D., and Edelman, E.R. (2004). Analysis of compartmental models of ligand-induced endocytosis. *J. Theor. Biol.* *229*, 127–138.
- Lakadamyali, M., Rust, M.J., and Zhuang, X. (2006). Ligands for clathrin-mediated endocytosis are differentially sorted into distinct populations of early endosomes. *Cell* *124*, 997–1009.
- Sheff, D.R., Daro, E.A., Hull, M., and Mellman, I. (1999). The receptor recycling pathway contains two distinct populations of early endosomes with different sorting functions. *J. Cell Biol.* *145*, 123–139.
- Ciechanover, A., Schwartz, A.L., Dautry-Varsat, A., and Lodish, H.F. (1983). Kinetics of internalization and recycling of transferrin and the transferrin receptor in a human hepatoma cell line. Effect of lysosomotropic agents. *J. Biol. Chem.* *258*, 9681–9689.
- Camazine, S., Deneubourg, J., Franks, N., Sneyd, J., Theraulaz, G., and Bonabeau, E. (2001). *Self-Organization in Biological Systems* (Princeton, NJ: Princeton University Press).
- Prigogine, I., and Nicolis, G. (1977). *Self Organization in Non-Equilibrium Systems* (New York: J. Wiley and Sons).
- Poser, I., Sarov, M., Hutchins, J.R., Hériché, J.K., Toyoda, Y., Pozniakovskiy, A., Weigl, D., Nitzsche, A., Hegemann, B., Bird, A.W., et al. (2008). BAC TransgeneOmics: a high-throughput method for exploration of protein function in mammals. *Nat. Methods* *5*, 409–415.
- von Schmoluchowski, M. (1917). Drei vorträge über diffusion Brownsche molekular bewegung und koagulation von kolloidteilchen. *Phys. Z.* *17*, 557–571.
- Hogg, R., Healy, T.W., and Fuersten, D.W. (1966). Mutual coagulation of colloidal dispersions. *Trans. Faraday Soc.* *62*, 1638–1651.
- Ziff, R.M. (1980). Kinetics of polymerization. *J. Stat. Phys.* *23*, 241–263.
- Cates, M.E., and Candau, S.J. (1990). Statics and dynamics of surfactant micelles. *J. Phys. Condens. Matter* *2*, 6869–6892.
- Meakin, P. (1992). Droplet deposition growth and coalescence. *Rep. Prog. Phys.* *55*, 157–240.

36. Turner, M.S., Sens, P., and Succi, N.D. (2005). Nonequilibrium raftlike membrane domains under continuous recycling. *Phys. Rev. Lett.* 95, 168301.
37. Christoforidis, S., McBride, H.M., Burgoyne, R.D., and Zerial, M. (1999). The Rab5 effector EEA1 is a core component of endosome docking. *Nature* 397, 621–625.
38. Horiuchi, H., Lippé, R., McBride, H.M., Rubino, M., Woodman, P., Stenmark, H., Rybin, V., Wilm, M., Ashman, K., Mann, M., and Zerial, M. (1997). A novel Rab5 GDP/GTP exchange factor complexed to Rabaptin-5 links nucleotide exchange to effector recruitment and function. *Cell* 90, 1149–1159.
39. Simonsen, A., Lippé, R., Christoforidis, S., Gaullier, J.-M., Brech, A., Callaghan, J., Toh, B.-H., Murphy, C., Zerial, M., and Stenmark, H. (1998). EEA1 links PI(3)K function to Rab5 regulation of endosome fusion. *Nature* 394, 494–498.